Future Energy
Open Access Journal
ISSN 2832-0328

February 2023| Volume 02 | Issue 01 | Pages 27-37

Journal homepage: https://fupubco.com/fuen

https://doi.org/10.55670/fpll.fuen.2.1.5

Future Publishing LLC

Article

Properties of turbulent non-premixed methane/air flames in a miniature-scale swirl burner under different coaxial airflow swirl numbers

Soroush Sheykhbaglou*[1]

[1]School of Mechanical, Aerospace, and Maritime Engineering, Amirkabir University of Technology (Tehran Polytechnic), No. 350, Hafez Ave, Tehran, Iran

ARTICLE INFO

Article history:
Received 24 August 2022
Received in revised form
24 September 2022
Accepted 30 September 2022

Keywords:
miniature swirl burner, flame lift-off,
flame characteristics,
intermittency distribution,
Otsu threshold, flame pulsating displacement

*Corresponding author
Email address:
soroush.sheykh@aut.ac.ir

DOI: 10.55670/fpll.fuen.2.1.5

ABSTRACT

This study investigates the dynamics and properties of non-premixed methane/air flames under three swirl numbers by segmenting flame images using the Otsu thresholding technique. Under three operating conditions, the lean blow out (LBO) and flame length, lift-off height, maximum width, flame angle, and flame pulsing displacements in terms of flame center of gravity, length, and width are measured and compared. A high-speed camera is used to record video of flames, and the image processing of frames collected from a high-speed video was accomplished by using the intermittency distribution method to quantitatively compare flame attributes. The findings show that increasing the swirl number from 0.5 to 0.7 generally has an unfavorable effect on the LBO at given fuel flow rates, and the LBO of flames under 35° (0.6 swirl number) and 40° (0.7 swirl number) swirlers has decreased up to about 15% and 40%, respectively when compared with a 30° swirler (0.5 swirl number). Additionally, observations indicate that the flame length (L) and lift-off height (LO) drop as the swirl number rises, although the flame width (W) and angle (α) show an ascending tendency. Besides, flame lift-off reveals an increasing-decreasing trend with an increment in the airflow, and flame length decreases as the airflow rate increases. It was also observed that flame pulsating displacements in terms of center of gravity (δ_{CG}), length (δ_L), and width (δ_W) increases with an increase in the fuel flow rate, and as the swirl number is increased, δ_{CG} and δ_L lessens, while δ_W increases.

1. Introduction

Image segmentation is a key step that enables feature extraction and identification in the field of image analysis and processing. Several techniques are used to perform the segmentation task: (1) threshold-based methods, (2) edge-based methods, (3) region-based methods, (4) clustering-based methods, (5) partial differential equation-based methods, and (6) artificial neural network-based methods [1]. Thresholding-based approaches are the most often used segmentation techniques among them because they are straightforward, simple to grasp, and easy to use [1, 2]. Combustion device design must take into account aspects such as flame form and size [3]. Threshold segmentation of pictures from photography and high-speed video recordings is a cheap and efficient way to obtain flame characteristics. Several relevant studies to obtain flame characteristics from image processing can be found in [4-12], which are generally based on the intermittency distribution approach. The flame height and lift-off of propane turbulent jet diffusion flames attenuated by carbon dioxide at ambient temperature and pressure were studied by Tao et al. [9]. They discovered that when CO_2 concentration increases, and the flame height drops. Additionally, it was shown that when CO_2 concentration rises, the flame lift-off height also rises.

The flame length of buoyant turbulent slot flames was examined by Gao et al. [13]. They created a rough prediction correlation for the length of the flame. They found that the flame length for the buoyancy-dominated and momentum-dominated flames is proportional to $(Fr_m)^{1/3}$ and $(Fr_m)^0$(modified Froude number that shows the relationship between initial speed and buoyancy), respectively. Zhou et al. [10] analyzed the flame height and lift-off height of rectangular fuel jet source fires. The flame buoyancy-momentum Froude number varied between 0.38 and 3.06. It was noticed that as the aspect ratio rises at a certain heat release rate, the flame height decreases. Zhang et al. [5] examined the features of curving flames in a tunnel model of a smaller size. They discovered that the recorded flame length under these conditions is almost comparable to that of flames in open space. In addition, they offered an empirical model for predicting the flame's tilt angle. Ligang et al. [14] measured the height of the coal jet flame using image processing. Image processing included the ROI (region of interest), filtering, grayscale, binarizing, and edge detection processes. The height of the flame was seen to decrease when the oxidizer temperature and main air velocity increased. Since swirl plays a significant role in flame stability, swirling flames are often used in practical combustion systems such as gas turbine engines and industrial burners [15, 16]. It is commonly acknowledged that swirl increases the local velocity fluctuations, hence increasing the turbulent burning velocity. Moreover, the swirl-induced recirculation zone may function as a heat source, causing heated products to interact with fresh reactants upstream [17]. Because of high energy density of hydrocarbon fuels, combustion-based micro-power devices are a more attractive option for portable power generation than rechargeable batteries [18-22]. In these systems, swirling flows are one method for flame stabilization [23-30]. To the best of authors' knowledge, there has never been research on the effects of swirl number on turbulent flame dynamics and characteristics by taking advantage of threshold-based image segmentation method. Using the Otsu threshold approach, this study compares the properties of turbulent swirling flames, including flame length, lift-off height, angle, maximum width, and pulsating displacements (in terms of flame center of gravity, length, and width), for three swirl numbers.

2. Experimental setup

Figure 1(a) depicts the experimental setup and flow delivery system layout. Air and Fuel are supplied by an air compressor and a high-pressure cylinder, respectively, and their pressures are then regulated using pressure reduction valves. Methane was used as fuel, and AZBIL MPC0020 and KOBOLD DMS-5 mass flow controllers with 1% full-scale accuracy regulate the flow of air and methane, respectively. Images of flames were taken with a Nikon V1 camera in its high-speed mode (400 fps) with a resolution of 640 × 240, a f-number of F/2.8, and a sensitivity of Hi 1. The miniature-scale burner employed in this study is illustrated in Figure 1(b). The core component of the burner is its axial flat vane swirlers which are made of polylactic acid (PLA). The construction of these swirlers was met using additive manufacturing techniques, and their geometrical characteristics are presented in Table 1. This burner's fuel nozzle consists of five 1 mm holes that are encircled by coaxial air. 3D-printed flat vane axial swirler are used to swirl coaxial air. Beer and Chigier proposed the following equation to get the well-known dimensionless theoretical swirl number for a swirler with a constant vane angle [23]:

$$S_n = \frac{2}{3}\frac{1-\left(\frac{D_h}{D_{sw}}\right)^3}{1-\left(\frac{D_h}{D_{sw}}\right)^2}\tan\theta \quad (1)$$

where D_h is the swirler hub diameter, D_{sw} is the swirler diameter, and θ is the vane angle from the centerline.

Table 1. Specifications of studied swirlers

Swirler No.	Vane angle, θ, (°)	Swirl number, S_n, (−)
1	30	0.5
2	35	0.6
3	40	0.7
No. of vanes: 10 Vane thickness: 0.5 mm Hub diameter, D_h: 4.5 mm Tip diameter, D_{sw}: 6.5 mm Swirl direction: counter-clockwise		

3. Results and discussion

In this section, the flame lean blowout limits, flame characteristics, including flame length, lift-off height, maximum width, flame angle, and flame pulsing displacements in terms of flame center of gravity, length, and width are measured and compared under three coaxial airflow swirl numbers and three operating conditions (Table 2).

Table 2. Experimental conditions

Case	Airflow rate, ($slpm$)	Methane flow rate, ($slpm$)	Coaxial airflow swirl number, S_n, (−)
1	3.0	0.100	0.5
2	3.0	0.150	0.5
3	3.0	0.200	0.5
4	3.0	0.100	0.6
5	3.0	0.150	0.6
6	3.0	0.200	0.6
7	3.0	0.100	0.7
8	3.0	0.150	0.7
9	3.0	0.200	0.7

3.1 Lean blowout (LBO) limits

In the present study, flame lean blowout limits are determined according to [12, 24]: (1) initially, a sustained diffusion flame is produced at a predetermined fuel flow rate, while the airflow rate is maintained at its minimum; (2) Second, the airflow rate is increased by 0.1 slpm while the fuel flow rate stays constant until the flame is extinguished; (3) The airflow rate at which the flame blows out (extingushes) is the lean blow out limit for the adjusted fuel flow rate; (4) This process is performed three times, and the average values are provided in this paper.

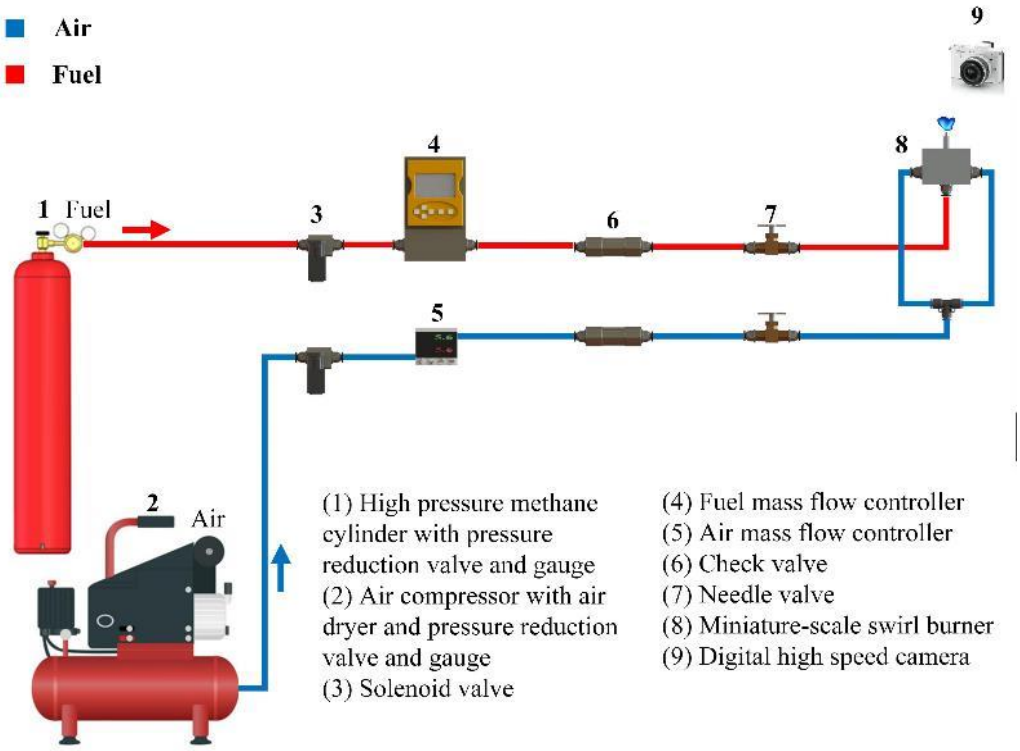

(a)

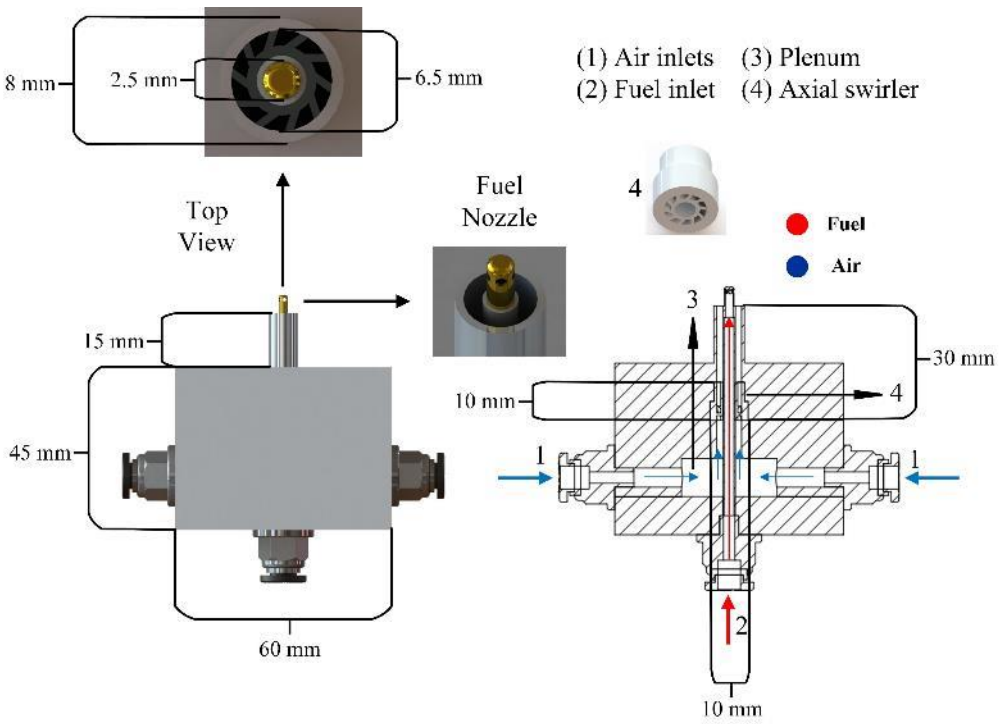

(b)

Figure 1. (a) Experimental setup and flow delivery system, (b) miniature-scale swirl burner

Figure 2(a) compares LBO values for three swirl numbers of 0.5, 0.6, and 0.7 for methane flow rates ranging from 0.050 to 0.500 slpm with an increment of 0.050 slpm. It has been seen that the equivalence ratio at which the flame blows out rises as the fuel flow rate is increased. It has also been seen that increasing the swirl number from 0.5 to 0.7 generally has an unfavorable effect on the LBO at given fuel flow rates (the flame blows out at lower airflow rates or higher equivalence ratio). This can be attributed to the following factors: (a) interaction between flame base and fuel nozzle due to an increase in the recirculation zone; (b) entrainment of cold outside air due to the recirculation zone; and (c) flame cooling due to an increase in the rate of strain on the flame with increasing swirl strength. In order to properly examine the impacts of raising the coaxial airflow swirl number from 0.5 to 0.7 on LBO, the findings of Figure 2(a) are compared to 30° swirler using the following equation:

$$\text{Diff in } \Phi = \frac{\Phi_{35^\circ \text{ or } 40^\circ \text{ swirler}} - \Phi_{30^\circ \text{ swirler}}}{\Phi_{30^\circ \text{ swirler}}} \times 100\% \quad (2)$$

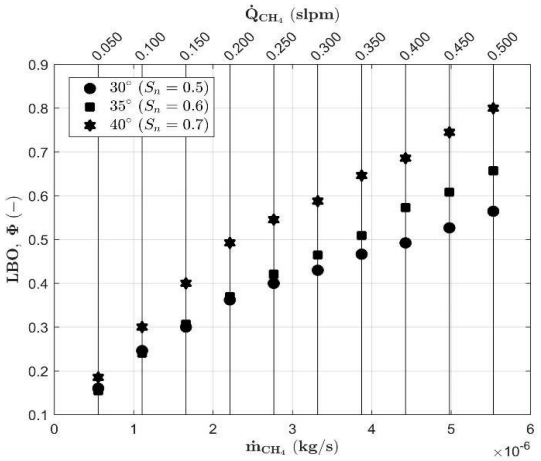

(a)

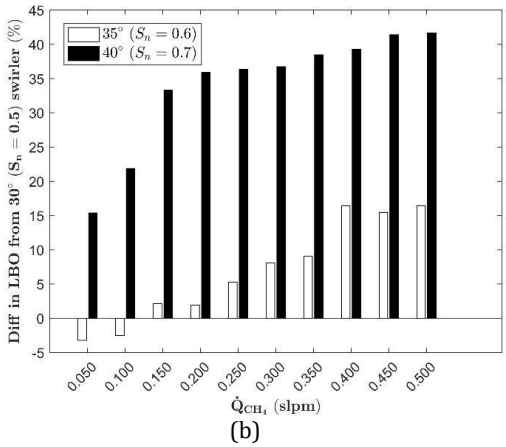

(b)

Figure 2. (a) Lean blow out (LBO), (b) percentage difference in LBO compared with 30° swirler

The percentage difference in the equivalence ratio at LBO under two swirl numbers is depicted in Figure 2(b). Negative and positive values indicate lower and higher equivalence ratios for LBO compared to 30° swirler, respectively. At two fuel flow rates of 0.050 and 0.100 slpm, a 35° swirler produces lower equivalence ratios for LBO. However, at fuel flow rates larger than 0.100 slpm, flames formed under swirl numbers of 0.6 and 0.7 blow out at higher equivalence ratios than flames formed under swirl number 0.5. For flames under 35° and 40°, the LBO has decreased up to about 15% and 40%, respectively.

3.2 Flame characteristics

In this section, the process for measuring is as follows: first, the fuel is introduced at predefined flow rates (0.100, 0.150, and 0.200), ignited, and a sustained diffusion flame is created for each swirler; second, the airflow rate is steadily raised until it achieves the desired value of 3; then, a Nikon V1 is used to record a high-speed video of the formed flame at 400 fps for 5 seconds, resulting in 2000 frames. Within the scope of this investigation, visual luminosity served as the indicator for flame contours. The objective was to more clearly depict form variations seen in flame photographs (not to get an accurate location of the reaction zone). Thresholding-based approach, which is the most common segmentation method because of its simplicity, ease of understanding, and implementation, is used to extract flame contours of an image [1, 2]. The intermittency distribution approach is used to examine and compare flame length, lift-off height, maximum width, and angle. This methodology has also been used in other research too [4-6, 9-11, 25]. In this procedure, the probability of a flame's existence is determined using the following steps: (a) 2000 frames are converted to grayscale and then preprocessed; (b) the Otsu thresholding algorithm, one of the most common methods in combustion, is applied to these grayscale images; (c) the thresholded images are binarized; (d) intermittency distribution is obtained by averaging the obtained images; (e) flame existence probability is obtained using a color bar (Figure 3 and the first row of Figure 5); (f) a threshold of 0.5 is applied to maintain the part with existence probability greater than 50%; (g) by converting the image coordinates to metric coordinates, flame length, lift-off height, maximum width, and angle are obtained (Figure 3). In Figure 4, quantitative comparisons of the flame's length (L), lift-off height (LO), maximum width (W), and angle (α) are shown for three different swirl numbers and operating conditions. In these figures, L, LO, and W are normalized to swirler diameter (D_sw). It is observed that the flame length and lift-off height drop as the swirl number rises, although the flame width and angle show an ascending tendency. Additionally, it has been shown that raising the methane flow rates causes an increase in these variables except for the flame angle. The radial mixing of air and fuel is improved and accelerated by increasing the swirl number, which also accelerates chemical processes. By moving the reaction zone upstream, swirl may also extend the residence duration during which reactants and products can coexist. As the swirl number rises, fuel can also be efficiently entrained. All of these may shorten the visible flame length as well the flame lift-off height. In addition, when the swirl number is rising, the flame width and angle increase because radial mixing is improved and the fuel and air mixture is pushed outward.

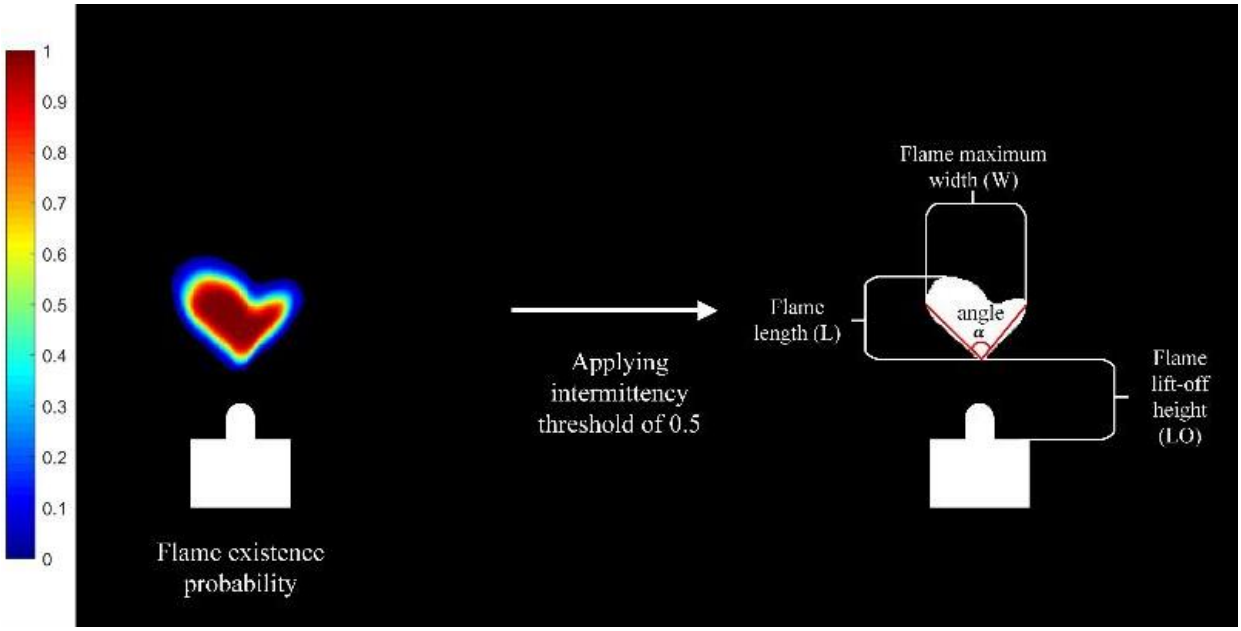

Figure 3. Definitions of flame length, lift-off height, maximum width, and angle

When the fuel flow rate is increased for swirling flames, the entrainment by swirling air diminishes owing to accelerated fuel velocity, resulting in more fuel burning in diffusion mode by the air from the surroundings. As a consequence, the flame lengthens, and its lift-off height increases with an increment in the fuel flow rate. On the other side, the fuel nozzle geometry may be responsible for the rise in flame width and angle with an increase in fuel flow rate. It is also observed that the flame lift-off height and angle exhibit the least sensitivity to an increase in fuel flow rate for a swirl number of 0.7. This is shown in Table 3, which was generated using MATLAB's curve-fitting toolbox with 95% confidence bounds (linear curve-fitting).

Table 3. Slopes of linear fitted curves for normalized flame lift-off and angle

Swirl number, S_n, (−)	LO/D_{sw} versus fuel flow rate	α versus fuel flow rate
0.5	1.662	−290.2
0.6	2.123	−273.3
0.7	0.7077	−189

Figure 5 depicts the mean flame shape (mean of 2000 frames for each operating condition) and its normalized intensity map as a function of the swirl number at 0.200 and 3 slpm methane and airflow rates, respectively. It has been shown that the bottom section of the flame has the greatest normalized intensity value, and by raising the swirl number, this area expands radially, the flame's width grows, and its length reduces. The mean flame contour (boundary) is obtained after applying the Otsu threshold to the grayscale mean flame and separating the foreground and background. The change of flame shape with airflow rate at a given fuel flow rate of 0.200 slpm for a 30° vane angle swirler (S_n=0.5) is shown in Figure 6 (single frames from 2000 frames of each operating condition is presented only). The following observations can be made:

Flame lift-off reveals an increasing-decreasing trend with an increment in the airflow rate, and the decreasing section corresponds to improved mixing of fuel and air because swirl has shown its effect. Flame length is affected by the airflow rate increase, and it decreases as the airflow rate increases. This is consistent with the findings in [26]. For swirling flames, this tendency is the consequence of an increase in turbulence intensity with an increase in airflow rate, which enhances fuel-air mixing and reduces flame length. At airflow rates, when flame lift-off has a declining trend, flame width reduces as airflow rate increases. This may be described as follows: when the swirl exerts its impact, a recirculation zone is created, which recirculates fuel and air, so decreasing the flame width. These findings are similar to other swirl numbers and operating conditions investigated in this research (Table 2).

In this investigation, the flame's center of gravity as well as its length and width, are used to examine flame fluctuations (pulsating displacements). The flame center is used to determine the position of the flame as a point utilizing the center of gravity concept (mass center in this case). Each pixel serves as a local point for calculating the mass center, and the intensity of each pixel represents its mass [27]. To obtain flame fluctuations, the Otsu threshold is used to generate binarized images of 2000 frames for each operating condition (boundaries of all 2000 frames are shown simultaneously in Figure 7 for methane and airflow rates of 0.200 and 3 *slpm*, respectively). The mean center of gravity ($x_{CG,mean}$, $y_{CG,mean}$), length (L_{mean}), and width (W_{mean}) are determined; then, the standard deviation is then used to calculate the flame's pulsating displacement in terms of the flame's center of gravity, length, and width [28]:

$$\delta_{CG} = \sqrt{\frac{\sum_{i=1}^{2000}\left[\left(x_{CG,i}-x_{CG,mean}\right)^2+\left(y_{CG,i}-x_{CG,mean}\right)^2\right]}{2000}} \quad (3)$$

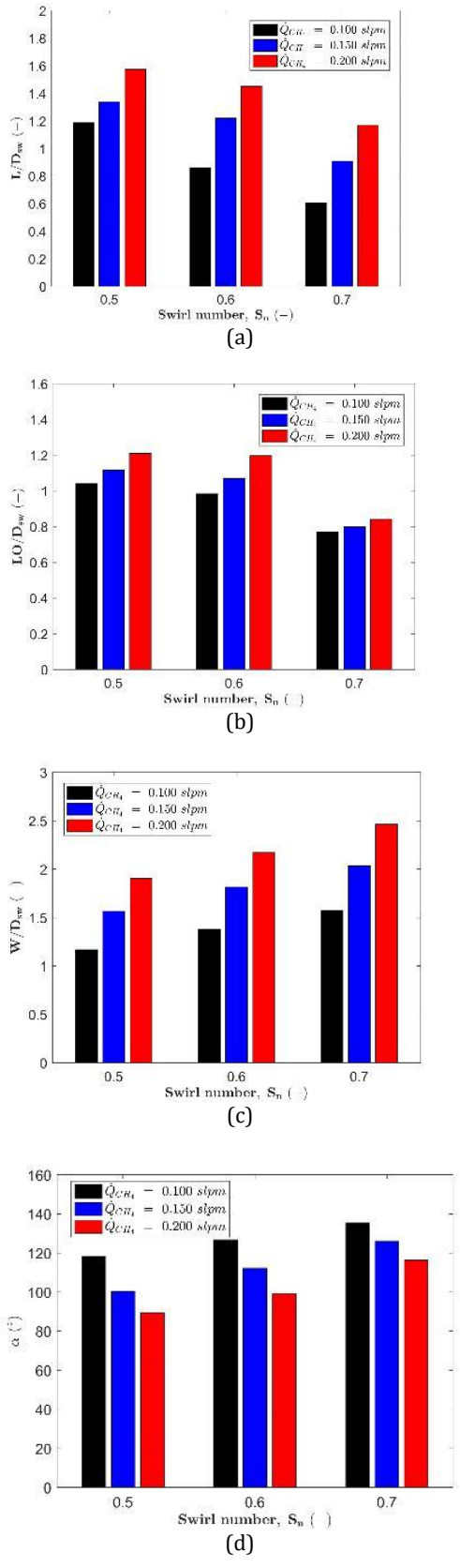

Figure 4. Normalized (a) flame length, (b) lift-off, (c) width, (d) angle as a function of swirl number

$$\delta_L = \sqrt{\frac{\sum_{i=1}^{2000}(L_i - L_{mean})^2}{2000}} \quad (4)$$

$$\delta_W = \sqrt{\frac{\sum_{i=1}^{2000}(W_i - W_{mean})^2}{2000}} \quad (5)$$

Where L_i and W_i stand for the length and maximum width of the i^{th} frame, respectively and $x_{CG,i}$ and $y_{CG,i}$ are the x and y coordinates of the i^{th} frame's center of gravity.

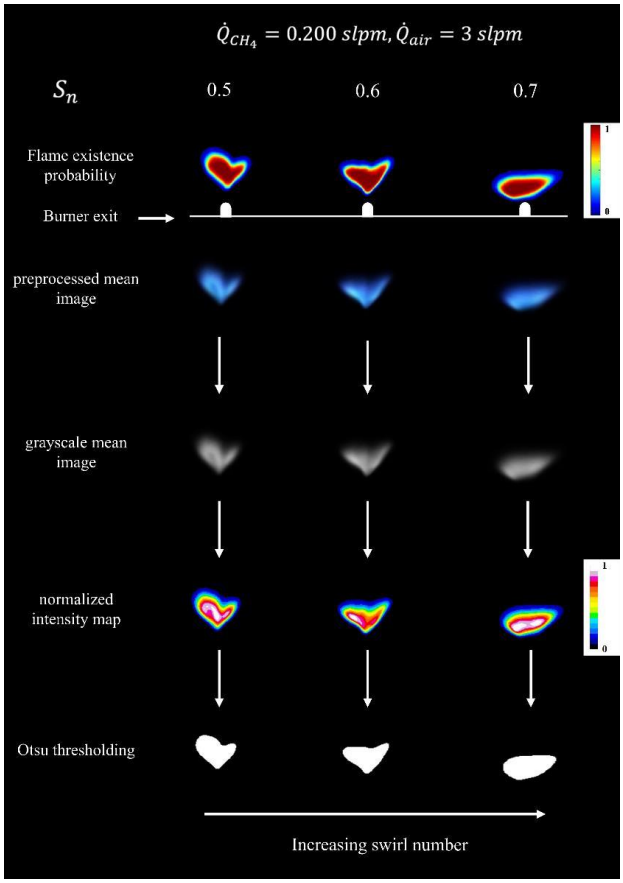

Figure 5. Flame existence probability, mean flame, its normalized intensity map, and its Otsu threshold versus swirl number at fuel and airflow rates of 0.200 and 3 slpm, respectively

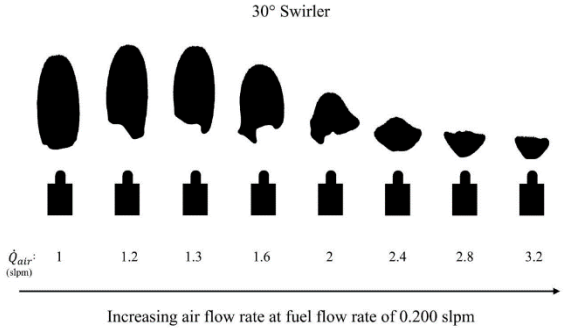

Figure 6. The change of flame shape with airflow rate at a given fuel flow rate of 0.200 slpm for a 30° vane angle swirler ($S_n = 0.5$)

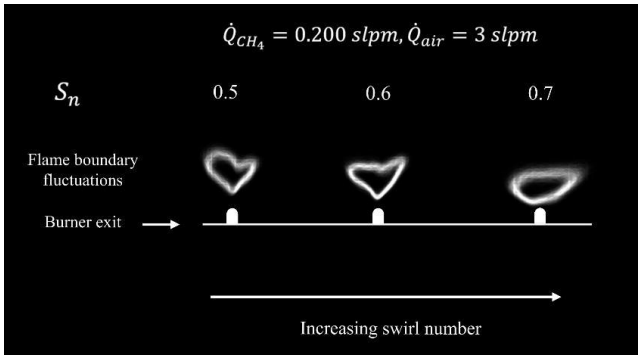

Figure 7. Fluctuations of flame boundary for methane and airflow rates of 0.200 and 3 slpm under three swirl numbers (obtained from 2000 frames for each experimental condition)

Figure 1 in Appendix I shows the flame length and width difference ($L_{diff} = |L_i - L_{mean}|, W_{diff} = |W_i - W_{mean}|$) over time spanning from 0 to 5 s. Observations reveal that when the swirl number rises, the peak values for flame length and width differences shift to lower and higher values, respectively. On each figure, the mean values of these differences are also displayed ($L_{diff,mean}$ and $W_{diff,mean}$). It is observed that as the swirl number is increased, $L_{diff,mean}$ and $W_{diff,mean}$ show a decreasing and increasing trend, respectively. This is presented quantitatively in Figure 2 in Appendix I. It is also noted from Figure 2 in Appendix I that these values ($L_{diff,mean}$ and $W_{diff,mean}$) rise when the fuel flow rate increases. The changes of δ_{CG}, δ_L, and δ_W with the swirl number at three fuel flow rates are determined and depicted in Figure 3 in Appendix I based on the above-mentioned formulae for quantifying flame fluctuations. It is noticed that flame pulsating displacements in terms of center of gravity (δ_{CG}), length (δ_L), and width (δ_W) increases with an increase in the fuel flow rate; although the increase in δ_{CG} from 0.6 swirl number to 0.7 swirl number is negligible. Additionally, it has been shown that as the swirl number is increased, δ_{CG} and δ_L lessens, while δ_W increases.

4. Conclusion

The In this work, turbulent non-premixed methane/air flame dynamics, and properties in a miniature-scale swirl burner were investigated under three different swirl numbers using high-speed video recordings of swirling flames. For the measurement of flame length, lift-off height, maximum width, and angle, an intermittency distribution approach based on the Otsu threshold method for image segmentation was used. Furthermore, the flame's center of gravity as well as its length and width, are used to examine flame fluctuations (pulsating displacements). The following are the main conclusions:

- Increasing the swirl number from 0.5 to 0.7 has an unfavorable effect on the lean blowout (LBO) at a given fuel flow rate (the flame blows out at lower airflow rates or higher equivalence ratio). This can be attributed to the interaction between flame base and fuel nozzle due to an increase in the recirculation zone, entrainment of cold outside air due to the recirculation zone, and flame cooling due to an increase in the rate of strain on the flame with increasing swirl strength. Additionally, for flames under 35° (0.6 swirl number) and 40° (0.7 swirl number) swirlers, the LBO has decreased up to about 15% and 40%, respectively, when compared with the 30° swirler (0.5 swirl number).
- Observations indicate that the flame length (L) and lift-off height (LO) drop as the swirl number rises, although the flame width (W) and angle (α) show an ascending tendency. Additionally, it has been shown that raising the methane flow rates causes an increase in these variables except for the flame angle. Additionally, Flame lift-off reveals an increasing-decreasing trend with an increment in the airflow rate at a specified methane flow rate, and the decreasing section corresponds to improved mixing of fuel and air because swirl has shown its effect. Besides, flame length is affected by the airflow rate increase, and it decreases as the airflow rate increases. For swirling flames, this tendency is the consequence of an increase in turbulence intensity with an increase in airflow rate, which enhances fuel-air mixing and reduces flame length.
- Flame pulsating displacements in terms of center of gravity (δ_CG), length (δ_L), and width (δ_W) increases with an increase in the fuel flow rate; although the increase in δ_CG from 0.6 swirl number to 0.7 swirl number is negligible. Additionally, it has been shown that as the swirl number is increased, δ_CG and δ_L lessens, while δ_W increases.

Ethical issue

The author is aware of and complies with best practices in publication ethics, specifically with regard to authorship (avoidance of guest authorship), dual submission, manipulation of figures, competing interests, and compliance with policies on research ethics. The author adheres to publication requirements that the submitted work is original and has not been published elsewhere in any language.

Data availability statement

All data that support the findings of this study are included within the article (and any supplementary files).

Conflict of interest

The authors declare no potential conflict of interest.

References

[1] Houssein EH, El-din Helmy B, Oliva D, Elngar AA, Shaban H. Multi-level Thresholding Image Segmentation Based on Nature-Inspired Optimization Algorithms: A Comprehensive Review. In: Oliva D, Houssein EH, Hinojosa S, editors. Metaheuristics in Machine Learning: Theory and Applications. Cham: Springer International Publishing; 2021. p. 239-65.

[2] Oliva D, Cuevas E. Digital Image Segmentation as an Optimization Problem. In: Oliva D, Cuevas E, editors. Advances and Applications of Optimised Algorithms in Image Processing. Cham: Springer International Publishing; 2017. p. 43-91.

[3] Xi Z, Fu Z, Hu X, Sabir SW, Jiang Y. An Investigation on Flame Shape and Size for a High-Pressure Turbulent Non-Premixed Swirl Combustion. Energies. 2018;11(4). doi: 10.3390/en11040930.

[4] Huang L, Liu C, Deng T, Jiang H, Wu P. Experimental investigation on the influence of central airflow on swirl combustion stability and flame shape. Journal of Thermal Analysis and Calorimetry. 2021;144(2):503-14. doi: 10.1007/s10973-020-10399-2.

[5] Zhang S, Cheng X, Zhu K, Yao Y, Shi L, Zhang H. Experimental study on curved flame characteristics under longitudinal ventilation in a subway tunnel. Applied Thermal Engineering. 2017;114:733-43. doi: https://doi.org/10.1016/j.applthermaleng.2016.12.023.
[6] Gao W, Liu N, Jiao Y, Xie X, Pan Y, Li Z, et al. Flame length of non-buoyant turbulent slot flame. Proceedings of the Combustion Institute. 2019;37(3):3843-50. doi: https://doi.org/10.1016/j.proci.2018.05.152.
[7] Sun X, Hu L, Ren F, Hu K. Flame height and temperature profile of window ejected thermal plume from compartment fire without facade wall. International Journal of Thermal Sciences. 2018;127:53-60. doi: https://doi.org/10.1016/j.ijthermalsci.2018.01.015.
[8] Xie K, Cui Y, Wang C, Cui G, Wang G, Qiu X, et al. Study on threshold selection method of continuous flame images of spray combustion in the low-pressure chamber. Case Studies in Thermal Engineering. 2021;26:101195. doi: https://doi.org/10.1016/j.csite.2021.101195.
[9] Tao C, Liu B, Dou Y, Qian Y, Zhang Y, Meng S. The experimental study of flame height and lift-off height of propane diffusion flames diluted by carbon dioxide. Fuel. 2021;290:119958. doi: https://doi.org/10.1016/j.fuel.2020.119958.
[10] Zhou Z, Chen G, Zhou C, Hu K, Zhang Q. Experimental study on determination of flame height and lift-off distance of rectangular source fuel jet fires. Applied Thermal Engineering. 2019;152:430-6. doi: https://doi.org/10.1016/j.applthermaleng.2019.02.094.
[11] Maynard TB, Butta JW. A Physical Model for Flame Height Intermittency. Fire Technology. 2018;54(1):135-61. doi: 10.1007/s10694-017-0678-7.
[12] Sheykhbaglou S, Robati SM. Effects of coaxial airflow swirl number on combustion and flame characteristics of methane/air and n-butane/air flames in a miniature-scale swirl burner. Engineering Research Express. 2022;4(2):025045. doi: http://dx.doi.org/10.1088/2631-8695/ac77dc.
[13] Gao W, Liu N, Jiao Y, Xie X, Pan Y, Li Z, et al. Flame length of buoyant turbulent slot flame. Proceedings of the Combustion Institute. 2019;37(3):3851-8. doi: https://doi.org/10.1016/j.proci.2018.05.153.
[14] Zheng L, Yu M, Yu S, Lu C. Measurement of Flame Height by Image Processing Method. Advanced Materials Research. 2011;301-303:983-8. doi: 10.4028/www.scientific.net/AMR.301-303.983.
[15] Liu T, Bai F, Zhao Z, Lin Y, Du Q, Peng Z. Large Eddy Simulation Analysis on Confined Swirling Flows in a Gas Turbine Swirl Burner. Energies. 2017;10(12). doi: 10.3390/en10122081.
[16] O'Connor J, Lieuwen T. Recirculation zone dynamics of a transversely excited swirl flow and flame. Physics of Fluids. 2012;24. doi: 10.1063/1.4731300.
[17] Feikema D, Chen R-H, Driscoll JF. Enhancement of flame blowout limits by the use of swirl. Combustion and Flame. 1990;80(2):183-95. doi: https://doi.org/10.1016/0010-2180(90)90126-C.
[18] Fernandez-Pello AC. Micropower generation using combustion: Issues and approaches. Proceedings of the Combustion Institute. 2002;29(1):883-99. doi: https://doi.org/10.1016/S1540-7489(02)80113-4.
[19] Ju Y, Cadou C, Maruta K. Microscale Combustion and Power Generation. Momentum Press; 2014.
[20] Kyritsis DC, Roychoudhury S, McEnally CS, Pfefferle LD, Gomez A. Mesoscale combustion: a first step towards liquid fueled batteries. Experimental Thermal and Fluid Science. 2004;28(7):763-70. doi: https://doi.org/10.1016/j.expthermflusci.2003.12.014
[21] Maruta K. Micro and mesoscale combustion. Proceedings of the Combustion Institute. 2011;33(1):125-50. doi: https://doi.org/10.1016/j.proci.2010.09.005.
[22] Sheykhbaglou S, Robati SM. Development of a small power generation system with a miniature-scale swirl burner, controlled heat transfer, and thermoelectric generators. Engineering Research Express. 2022;4(2):025006. doi: https://doi.org/10.1088/2631-8695/ac6281.
[23] Lefebvre AH, Ballal DR. Gas Turbine Combustion: Alternative Fuels and Emissions, Third Edition. Taylor & Francis; 2010.
[24] Alsulami R, Windom B. Liquid Jet Fuel Property Impacts on Combustion Performance. Journal of Propulsion and Power. 2020;37. doi: 10.2514/1.B38209.
[25] Sheykhbaglou S, Karami S. Comparative study on threshold selection for measuring characteristics of turbulent swirling flames in a miniature-scale swirl burner. Signal, Image and Video Processing. 2022. doi: 10.1007/s11760-022-02344-7.
[26] Patel V, Shah R. Experimental investigation on flame appearance and emission characteristics of LPG inverse diffusion flame with swirl. Applied Thermal Engineering. 2018;137:377-85. doi: https://doi.org/10.1016/j.applthermaleng.2018.03.105.
[27] Yoon J, Kim M-K, Hwang J, Lee J, Yoon Y. Effect of fuel–air mixture velocity on combustion instability of a model gas turbine combustor. Applied Thermal Engineering. 2013;54(1):92-101. doi: https://doi.org/10.1016/j.applthermaleng.2013.01.032.
[28] Xiong C, Liu Y, Fan H, Huang X, Nakamura Y. Fluctuation and extinction of laminar diffusion flame induced by external acoustic wave and source. Scientific Reports. 2021;11(1):14402. doi: https://doi.org/10.1038/s41598-021-93648-0.

Appendix I

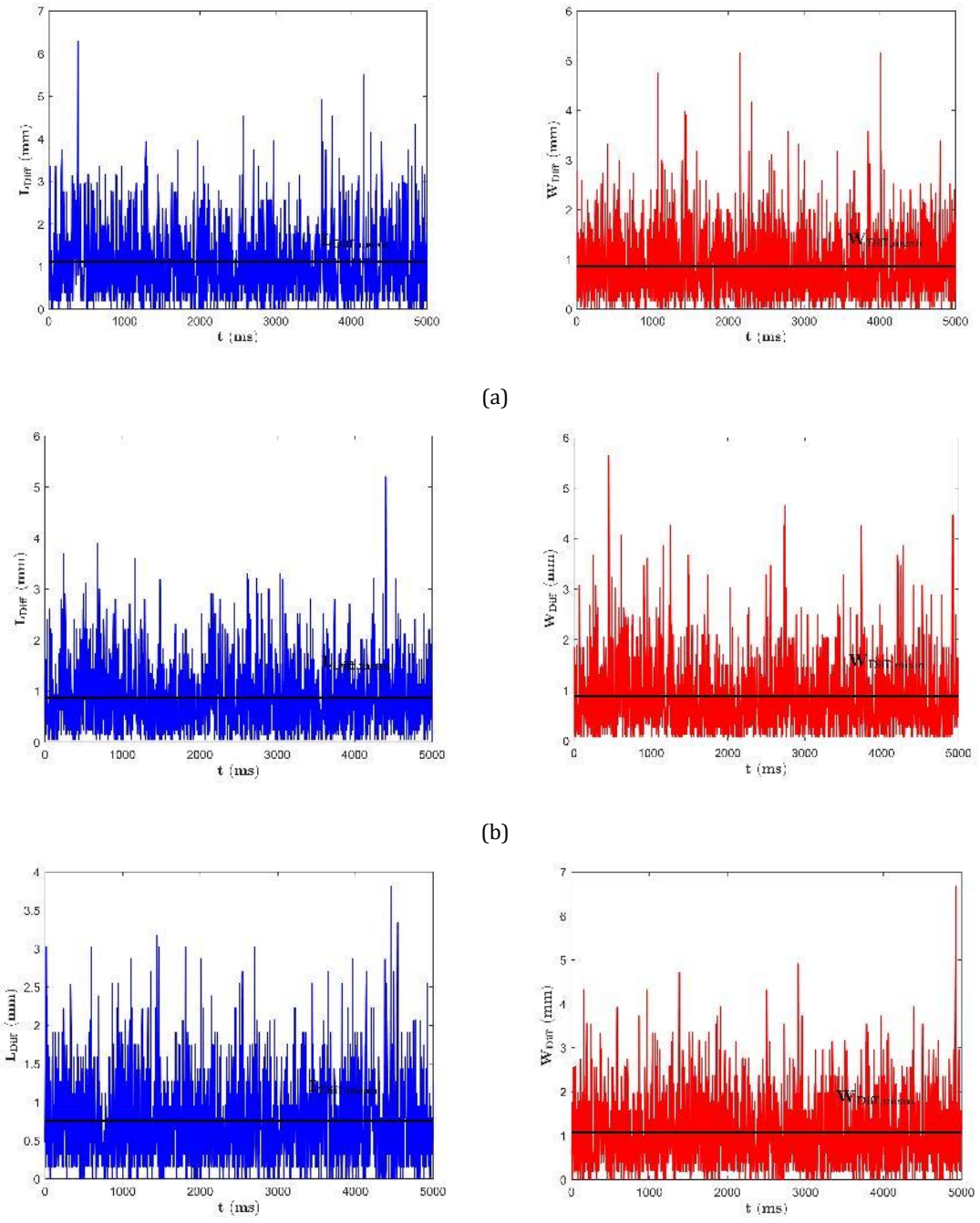

Figure 1. Fluctuations of flame length and width differences with time (2000 frames in 5 seconds) for methane and airflow rates of 0.200 and 3 slpm under three swirl numbers: (a) 30°; (b) 35°; (c) 40°.

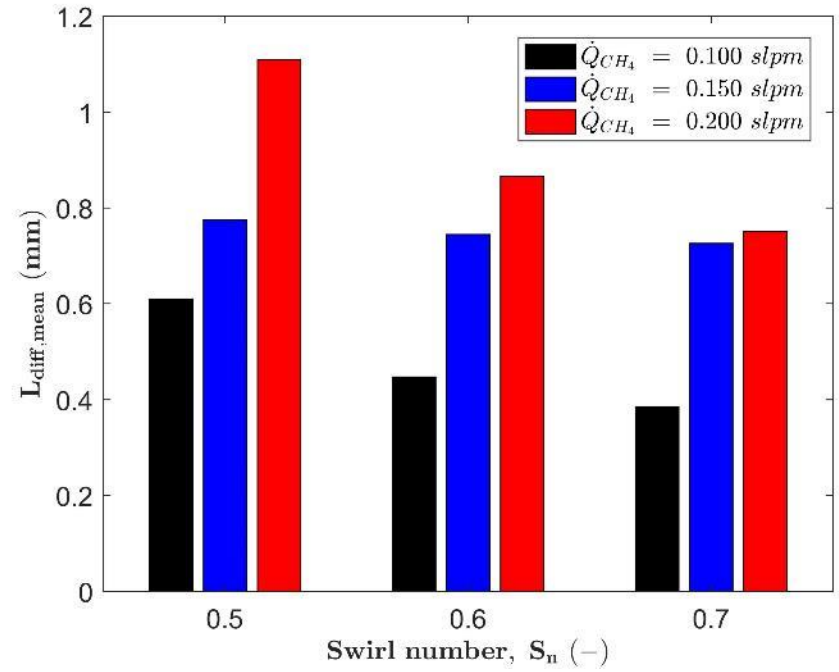

(a)

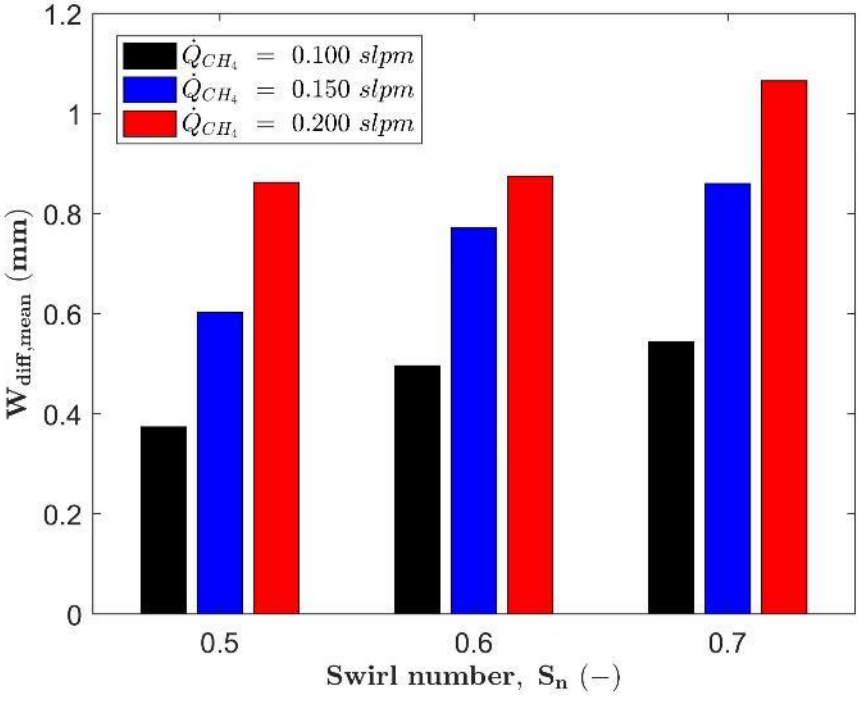

(b)

Figure 2. (a) $L_{diff,mean}$ and (b) $W_{diff,mean}$ as a function of swirl number at three fuel flow rates of 0.100, 0.150, and 0.200 slpm at the airflow rate of 3 slpm

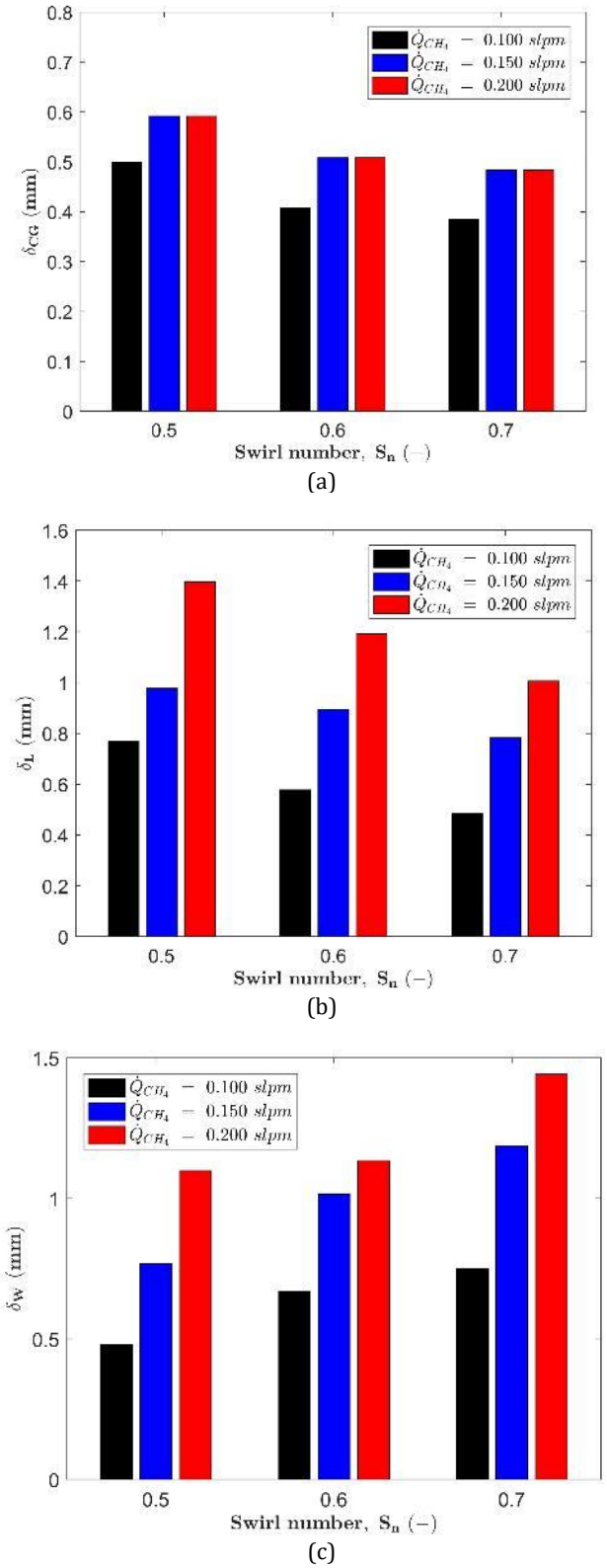

Figure 3. Flame pulsating displacements in terms of (a) center of gravity, (b) length, and (c) width as a function of swirl number at three fuel flow rates of 0.100, 0.150, and 0.200 slpm and at the airflow rate of 3 slpm